Journal of Physics: Conference Series **496** (2014) 012010 doi:10.1088/1742-6596/496/1/012010

Coulomb crystals in neutron star crust

D. A. Baiko

A.F. Ioffe Physical Technical Institute, Saint-Petersburg, Russian Federation

E-mail: baiko@astro.ioffe.ru

Abstract. It is well known that neutron star crust in a wide range of mass densities and temperatures is in a crystal state. At a given density, the crystal is made of fully ionized atomic nuclei of a single species immersed in a nearly incompressible (i.e., constant and uniform) charge compensating background of electrons. This model is known as the Coulomb crystal model. In this talk we analyze thermodynamic and elastic properties of the Coulomb crystals and discuss various deviations from the ideal model. In particular, we study the Coulomb crystal behavior in the presence of a strong magnetic field, consider the effect of the electron gas polarizability, outline the main properties of binary Coulomb crystals, and touch the subject of quasi-free neutrons permeating the Coulomb crystal of ions in deeper layers of neutron star crust.

1. Introduction

Coulomb crystals are expected to form in such astrophysical objects as cores of white dwarfs and crusts of neutron stars. At a given density, the crystal is made of fully ionized atomic nuclei of a single species (with charge Ze, mass M, and number density n) immersed in a nearly incompressible (i.e., constant and uniform) charge compensating background of electrons. In this paper we review the structure, thermodynamics, and elastic properties of Coulomb crystals and discuss a number of modifications of the ideal Coulomb crystal model. In particular, we consider realistic (i.e., polarizable) electron background, analyze Coulomb crystal behavior in a strong magnetic field, and study ordered binary Coulomb crystal mixtures.

Let us recall the structure of the crust of a not too hot neutron star or an old white dwarf (e.g., [1]). On the top, there is a region composed of partially ionized atoms and non-degenerate electrons. As one goes deeper, the electrons form strongly degenerate gas, that to a good approximation can be treated as a uniform charge-neutralizing background, while ions get completely ionized by electron pressure. At densities greater than 10^6 g cm^{-3} electrons become relativistic. Central densities of white dwarfs are $\lesssim 10^{10}$ g cm^{-3}. Yet even deeper, above the neutron drip density of $\sim 4\cdot 10^{11}$ g cm^{-3}, the atomic nuclei become extremely neutron-rich and, in addition to nuclei and electrons, free neutrons appear. These neutrons are most likely superfluid and they practically play no role in our considerations. Finally, at densities greater than 10^{14} g cm^{-3}, the atomic nuclei acquire non-spherical shapes, start touching each other, and form the so-called region of nuclear pasta. In this work, we shall limit ourselves to the intermediate regions and exclude the partially ionized and nuclear pasta phases.

2. Review of thermodynamic and elastic properties

Ideal Coulomb crystal is expected to have a body-centered cubic (bcc) lattice, which is thermodynamically preferable at all temperatures (below melting). The lattice phonon wave


Content from this work may be used under the terms of the Creative Commons Attribution 3.0 licence. Any further distribution of this work must maintain attribution to the author(s) and the title of the work, journal citation and DOI.
Published under licence by IOP Publishing Ltd

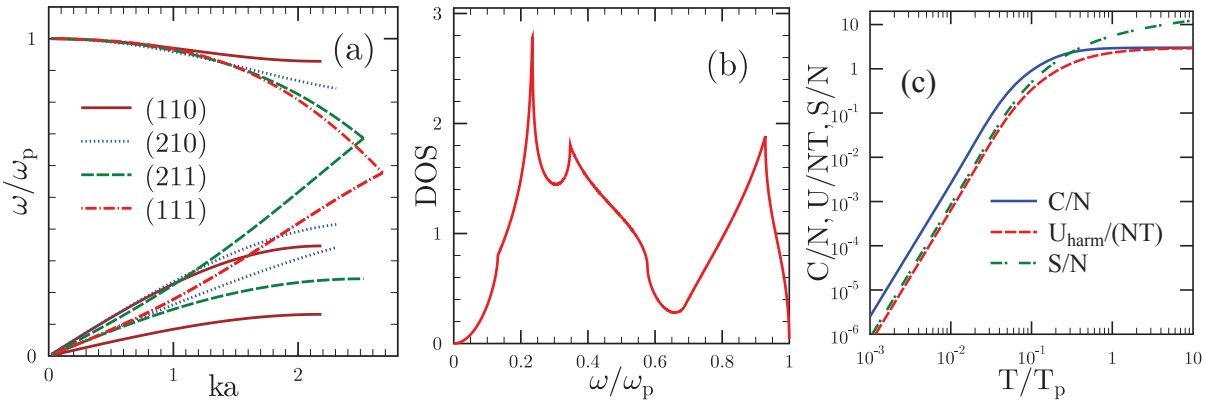

Figure 1. (a) Phonon dispersion curves in 4 directions of the wave vector vs. ka (cf. Fig. 2a for our direction specification convention), where $a = (4\pi n/3)^{-1/3}$ is the ion sphere radius; (b) density of phonon states; (c) specific heat, energy, and entropy of the Coulomb bcc lattice.

vectors $\mathbf{k}$ are restricted to its first Brillouin zone (BZ), which has the shape of a rhombic dodecahedron. To study crystal thermodynamics one needs to find phonon frequencies ω on a dense $\mathbf{k}$-grid in the BZ. These are solutions of a secular equation $\det\{D^{\alpha\beta}(\mathbf{k}) - \omega_i^2(\mathbf{k})\delta^{\alpha\beta}\} = 0$, where $D^{\alpha\beta}(\mathbf{k})$ is the dynamic matrix. The tricky part about Coulomb crystals is that one needs to take into account interactions of a given ion with all other ions (not just with the nearest neighbors) when constructing the dynamic matrix. At any wave vector $\mathbf{k}$ in the BZ there are 3 phonon modes (cf. Fig. 1a). In each direction 2 modes are acoustic ($\omega_{1,2} \propto k$ as $k \to 0$; in certain high symmetry directions these 2 modes coincide), while the third one is optic ($\omega_3 \to \omega_\mathrm{p}$ as $k \to 0$). At any $\mathbf{k}$ the phonon frequencies satisfy the Kohn's sum rule $\sum_{i=1}^{3} \omega_i^2 = \omega_\mathrm{p}^2$, where $\omega_\mathrm{p} = \sqrt{4\pi n Z^2 e^2/M}$ is the ion plasma frequency.

In Fig. 1b we show the phonon density of states (DOS) $\nu(x)$ (where $x \equiv \omega/\omega_\mathrm{p}$) of the ideal Coulomb bcc lattice [2]. By definition DOS is the fraction of phonon states per unit interval of frequencies. At $x \to 0$, DOS depends quadratically on x, which is a well-known sign of the presence of acoustic phonons. There are points where the derivative of DOS becomes infinite. These are the Van Hove singularities associated with saddle points of the frequency dependence on $\mathbf{k}$. For the Coulomb crystal there is no forbidden gap between acoustic and optic phonons.

Consider the ideal Coulomb crystal energy. Its part related to ions can be subdivided into 4 terms $E = U_\mathrm{M} + E_\mathrm{0ph} + U_\mathrm{harm} + U_\mathrm{anharm}$. In this case, U_M is the electrostatic (Madelung) energy of static ions and neutralizing background, $E_\mathrm{0ph} + U_\mathrm{harm}$ is the phonon energy, in which one can distinguish the zero-point, E_0ph, and the thermal, U_harm, contributions, and U_anharm is the anharmonic energy. The latter can be important, but is neglected for the purpose of this work. Also neglected are the energy of the electron gas alone, which is the same for any crystal structure, and the polarization correction to the electron-ion interaction energy (see Sect. 3). Phonon thermodynamic quantities are given either by three-dimensional BZ integrals or by one-dimensional integrals with the DOS and can be computed numerically [3, 4]. For instance,

$$U_\mathrm{harm} = \sum_{\mathbf{k}i} \frac{\hbar\omega_i(\mathbf{k})}{e^{\hbar\omega_i(\mathbf{k})/T} - 1} = 3N\hbar\omega_\mathrm{p} \int_0^\infty \frac{x\nu(x)\mathrm{d}x}{\exp(x/t) - 1}\,, \qquad (1)$$

where $t = T/T_\mathrm{p}$ and $T_\mathrm{p} = \hbar\omega_\mathrm{p}$ is the ion plasma temperature. The lattice specific heat $C/N = \mathrm{d}(U_\mathrm{harm}/N)/\mathrm{d}T$, energy $U_\mathrm{harm}/(NT)$, and entropy S/N are illustrated in Fig. 1c. At high T, $C/N \approx 3$ (Dulong-Petit law) and at low T, $C \propto T^3$ according to the Debye law.

Let us outline the calculation of the Coulomb crystal elastic moduli. Suppose one applies an infinitesimal uniform deformation to the crystal $R_\alpha \to R_\alpha + u_{\alpha\beta}R_\beta$, where $\mathbf{R}$ are lattice vectors and $u_{\alpha\beta}$ are small constant displacement gradients, Fig. 2a (arrows in this plot show our

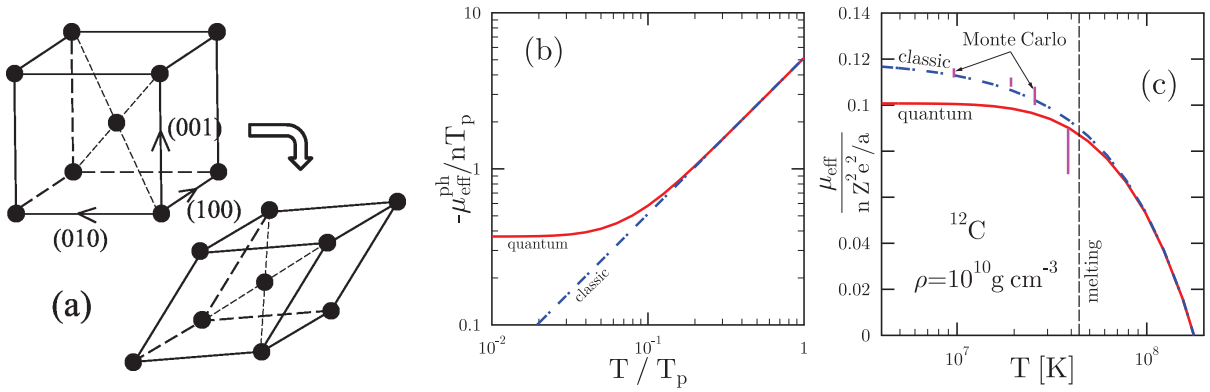

Figure 2. (a) Bcc lattice structure before and after a uniform deformation; (b) phonon contribution to the effective shear modulus; (c) total effective shear modulus.

specification convention for vector directions). The electrostatic energy of the deformed lattice can be expanded in powers of $u_{\alpha\beta}$. The zero-order term is the Madelung energy, the linear term is the electrostatic pressure times the volume change, and the coefficients of the quadratic terms are various static lattice elastic moduli. All these quantities have been found by Fuchs [5].

The potential energy of harmonic lattice vibrations can be also expanded in powers of $u_{\alpha\beta}$, which results in the phonon Hamiltonian $\hat{H}_{\rm ph} = \hat{H}_0 + \delta\hat{H}$. In this case $\hat{H}_0$ is the standard (nondeformed) expression $\hat{H}_0 = \sum_{\mathbf{k}i} \hbar\omega_{\mathbf{k}i}(0.5 + a^\dagger_{\mathbf{k}i}a_{\mathbf{k}i})$ and

$$\delta\hat{H} = 0.5\sum_{\mathbf{k}ii'}\left(\Phi^{\mathbf{k}ii'}_{\alpha\beta}\,u_{\alpha\beta} + 0.5\,\Phi^{\mathbf{k}ii'}_{\alpha\beta\gamma\lambda}u_{\alpha\beta}u_{\gamma\lambda}\right)(a_{\mathbf{k}i} + a^\dagger_{-\mathbf{k}i})(a_{-\mathbf{k}i'} + a^\dagger_{\mathbf{k}i'})\ , \qquad (2)$$

where $a^\dagger$ and a are the phonon creation and annihilation operators, while the quantities Φ are closely related to derivatives of the dynamic matrix [6]. The term $\delta\hat{H}$ should now be treated as a perturbation and the respective change of the crystal free energy can be found with the aid of the thermodynamic perturbation theory (e.g., [7]). Expanding the free energy in powers of $u_{\alpha\beta}$ one obtains phonon contributions to crystal elastic moduli as the quadratic term coefficients [6]. It is worth mentioning that in this way the quantization of ion motion is naturally included.

In isotropic matter there are only 2 independent elastic moduli, the compressibility modulus K and the shear modulus μ (e.g., [8]). In cubic crystals there are 3 independent elastic coefficient (e.g., [9]). However, we do not expect the neutron star crust to represent a single crystal. Likely, there are small domains with various orientations of the crystal axes and the matter is "effectively" isotropic. To describe this we follow an isotropisation procedure for the elastic coefficients proposed in [10] and obtain an effective shear modulus of the crystal $\mu_{\rm eff}$.

In Fig. 2b we plot the phonon contribution to the effective crystal shear modulus. It is negative and it grows in magnitude with temperature. As expected, excitation of phonons reduces the shear modulus and the crystal resistance to the shear stress. At low T a quantum effect is observed. The phonon contribution does not disappear even at $T = 0$. It saturates at a constant negative value associated with zero-point vibrations. The total crystal shear modulus

$$\mu_{\rm eff} = \mu^{\rm static}_{\rm eff} + \mu^{\rm ph}_{\rm eff} = 0.1194\,nZ^2e^2/a - n\hbar\omega_{\rm p}\left[0.05008 + 136.6(T/T_{\rm p})^3\right]^{1/3}\ . \qquad (3)$$

It has 2 contributions, the static lattice part proportional to the typical Coulomb energy Z^2e^2/a and the phonon part proportional to the typical phonon energy $\hbar\omega_{\rm p}$. In Fig. 2c we show the total effective shear modulus of carbon at 10^{10} g cm^{-3} as a function of temperature. The bars (1σ) represent classic Monte-Carlo (MC) results from [10]. The dot-dashed (blue) line is our analytic calculation without quantum effects (cf. dot-dashed curve in Fig. 2b). It describes the bars reasonably well. The solid (red) line is our more accurate results with quantum effects included.

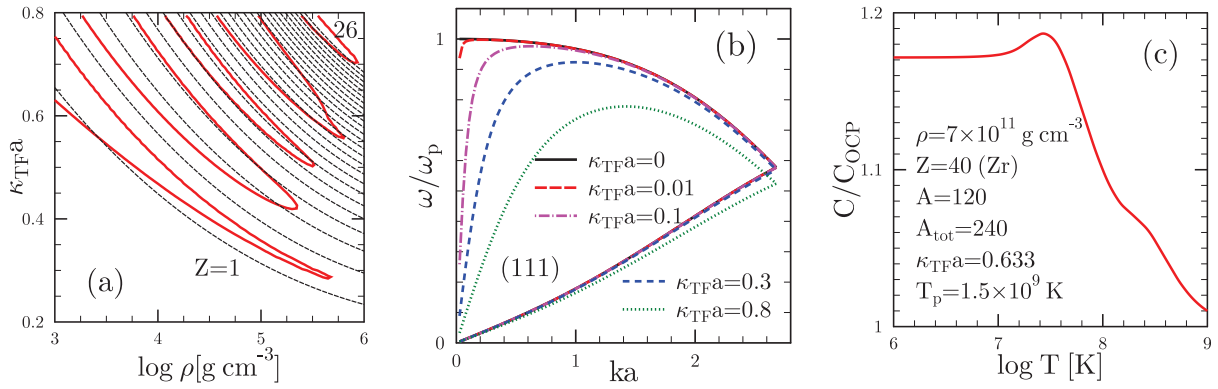

Figure 3. (a) Contours of zero energy difference between bcc and fcc lattices at $T = 0$; (b) phonon dispersion curves for the TF model of polarizable electron background (note that lower acoustic branch curves for $\kappa_{TF}a = 0, 0.01, 0.1$ have merged); (c) ratio of phonon heat capacity with screening to that of the ideal Coulomb crystal (OCP).

3. Electron polarization

In reality the electron gas is not uniform. It is polarizable or, in other words, there is electron screening of the ion charge. This screening adds a term U_ϵ to the lattice energy, which is different for different crystal structures. It can be readily written in the linear response framework as

$$U_\epsilon = \frac{Z^2e^2}{2}\int \frac{\mathrm{d}\mathbf{q}}{(2\pi)^3}\frac{4\pi}{q^2}\left[\frac{1}{\epsilon(q)}-1\right]\left(\sum_{\mathbf{R}} e^{i\mathbf{qR}} - n\int \mathrm{d}\mathbf{r} e^{i\mathbf{qr}}\right), \qquad (4)$$

where $\epsilon(q)$ is the electron dielectric function. We study 2 models of the dielectric function, the simple Thomas-Fermi (TF) model $\epsilon_{TF}(q) = 1 + \kappa_{TF}^2/q^2$ and the more realistic RPA dielectric function of the degenerate relativistic electron gas ϵ_J obtained by Jancovici [11]. In this case $\kappa_{TF} = 2k_F\sqrt{\alpha/(\pi\beta)}$ is the TF wave number, which measures the screening strength, $\beta = v_F/c$, $\alpha = 1/137$, while v_F and k_F are the electron Fermi velocity and wave number. It is important to realize that the linear response formalism is strictly valid only for $\kappa_{TF}a \ll 1$.

First of all, if one adds the term U_ϵ to the energy, structural transitions appear [12]. Solid (red) lines in Fig. 3a correspond to zero energy difference between the face-centered cubic (fcc) and the bcc structures if the lattice energy is approximated as $U_M + U_\epsilon$. Inside the domains the fcc lattice is preferable at $T = 0$. Dashed lines are lines of constant charge from $Z = 1$ to $Z = 26$. The structural transitions appear only for the more realistic Jancovici dielectric function. Calculations with ϵ_{TF} always predict a lower energy for the bcc lattice.

The phonons in the crystal with electron screening are also different. In Fig. 3b we show dispersion curves calculated with ϵ_{TF} in the (111) direction of the BZ, where 2 acoustic modes coincide. The main effect is that the optic mode is converted into an acoustic one at wave vectors smaller than the TF wave number [13]. It is remarkable that there is virtually no difference between the dispersion curves calculated with the TF and Jancovici dielectric functions [12] and thus the TF description of the phonon modes is quite adequate (unlike U_ϵ).

Once the phonon frequencies are known, one can analyze various crystal thermodynamic functions. For instance, one can calculate and compare free energies of the fcc and bcc lattices to see whether the structural transitions exist at higher temperatures. It appears that at $T = T_p$ the bcc lattice is always preferable [12] and, therefore, the structural transitions may start happening at some point after solidification during the star cooling process.

Another example is the heat capacity. In Fig. 3c we show the ratio of the phonon heat capacities with and without electron screening (TF model) for zirconium in the inner neutron star crust at $\rho = 7 \cdot 10^{11}$ g cm^{-3}. At these high densities electrons are ultrarelativistic and the

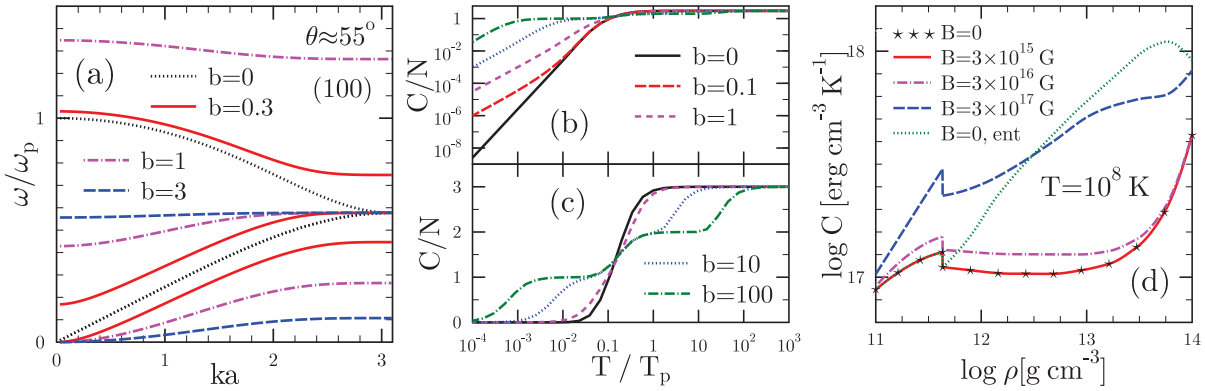

Figure 4. (a) Phonon dispersion curves of a magnetized crystal; (b) and (c) magnetized crystal specific heat in logarithmic and linear scales; (d) ion specific heat of magnetized inner neutron star crust.

screening parameter $\kappa_{\rm TF}a$ is determined only by Z. One sees that the background polarizability enhances the heat capacity in quantum regime but rather moderately (by about 20% at best). The reason for the increase is the conversion of the optic mode into the acoustic one, which can then be excited at arbitrarily low temperatures and contributes to the Debye T^3 asymptote.

4. Magnetized Coulomb crystal

Suppose the ideal Coulomb crystal is placed in an external uniform magnetic field. All results are weakly sensitive to the field direction. We assume that the field is directed towards one of the nearest neighbors, i.e. direction (111). The secular equation takes the form $\det\{D^{\alpha\beta}(\mathbf{k})-\omega_i^2(\mathbf{k})\delta^{\alpha\beta}-i\omega_i(\mathbf{k})\omega_{\rm B}\epsilon^{\alpha\gamma\beta}n^\gamma\}=0$, where $\mathbf{n}=\mathbf{B}/B$ and $\omega_{\rm B}=ZeB/(Mc)$ is the ion cyclotron frequency. The most important parameter turns out to be $b=\omega_{\rm B}/\omega_{\rm p}$. When $b\gg 1$ the magnetic field is really important and the crystal is said to be strongly magnetized.

It is very useful to recall a simple problem of a charged harmonic oscillator in a magnetic field (e.g., [14]). We have the obvious equation of motion $\ddot{\mathbf{r}}+\omega_0^2\mathbf{r}=\omega_{\rm B}\mathbf{v}\times\mathbf{n}$ with the Lorenz force on the right-hand side, ω_0 being the oscillator frequency in the absence of the field. Assuming the field is along the z-axis and introducing the new variable $\xi=x+iy$, we arrive at 2 equations: $\ddot{z}+\omega_0^2 z=0$ and $\ddot{\xi}+\omega_0^2\xi=-i\omega_{\rm B}\dot{\xi}$, from which we immediately get the eigenfrequencies of the magnetized system as $\omega_{1,3}=\sqrt{\omega_0^2+\omega_{\rm B}^2/4}\mp\omega_{\rm B}/2$ and $\omega_2=\omega_0$. If we assume now that the frequency ω_0 is that of an acoustic phonon, $\omega_0=ck$, and $\omega_{\rm B}\gg\omega_0$, we get 3 solutions, one of which (ω_1) depends on k quadratically and is $\propto 1/B$, another (ω_3) is at cyclotron frequency, so that it is $\propto B$, and the last one (ω_2) is independent of B. This simple picture is quite adequate for qualitative understanding of the magnetized crystal phonon spectrum.

Exact solution of the crystal secular equation [15] shows that the behavior of its phonon modes is qualitatively different for $\mathbf{kB}\neq 0$ and $\mathbf{kB}=0$. In the former case (see Fig. 4a, where the angle between $\mathbf{k}$ and $\mathbf{B}$ is $\approx 55^{\rm o}$) branch 1 has quadratic dependence on k at $k\to 0$, while branch 3 to a good accuracy is at the ion cyclotron frequency. Branch 2 is optic and sweeps the space between the upper acoustic field-free branch and the ion plasma frequency becoming B-independent at $b\gg 1$. The situation is different for $\mathbf{k}$ perpendicular to $\mathbf{B}$. In this case branches 1 and 2 remain acoustic, while branch 3 is optic. At any $\mathbf{k}$ the frequencies satisfy a modified Kohn's sum rule $\sum_{i=1}^3\omega_i^2=\omega_{\rm p}^2+\omega_{\rm B}^2$.

Once the phonon frequencies are known the magnetized crystal thermodynamic functions can be calculated via BZ integration using the same general formulas as in the field-free case [15, 16]. The most important feature of the magnetized crystal heat capacity is that the branch 1 contribution (and the total heat capacity) behaves as $T^{3/2}$ at low temperatures instead of the Debye T^3 law [17]. This is a direct consequence of the quadratic dependence of the branch

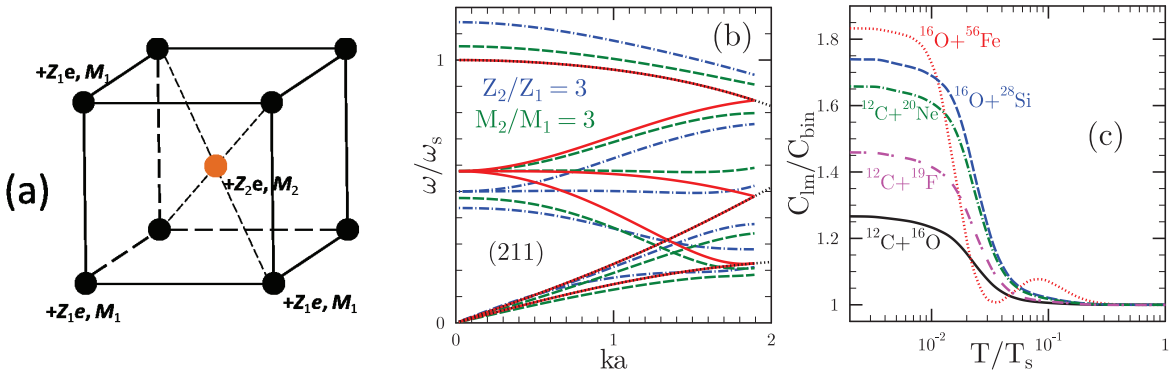

Figure 5. (a) Binary crystal structure; (b) binary crystal dispersion curves; (c) the ratio of binary crystal heat capacities obtained from the linear mixing theory and from the exact phonon spectrum.

frequency on k. Branch 2 contribution behaves as T^4 as a result of these phonons being acoustic only in the plane perpendicular to **B** and optic otherwise. Branch 3 heat capacity is exponentially suppressed at low T as a result of its optic nature. Consequently at low T the total specific heat of a strongly magnetized Coulomb crystal is bigger than that of the non-magnetized one by many orders of magnitude, Fig. 4b. At high T the specific heat has a peculiar staircase structure for strong magnetization, Fig. 4c. The reason is that the frequencies of the branches are very different ($\propto 1/B$, independent of B, and $\propto B$) and get saturated at very different temperatures.

Let us see if magnetization can modify the heat capacity of the inner neutron star crust [16], where practically all the crust mass is located. Curves in Fig. 4d show the total ion heat capacity as a function of mass density assuming the smooth composition model of ref. [1]. We see that the non-magnetized curve (stars) merges with the $B = 3 \cdot 10^{15}$ G curve (solid, red), while the $B = 3 \cdot 10^{16}$ G curve (dot-dashed, magenta) is somewhat above. In order to have a meaningful enhancement of the heat capacity at these high densities it is necessary to have a really huge field on the order of 10^{17} G (dashed, blue curve). If such fields exist in magnetars, this will be very important for their cooling models. At lower densities and temperatures in the external crust a smaller field will have a similar substantial effect, which should be important for the dynamics of bursts and superbursts as well as for afterburst relaxation modeling.

Recently, it has been argued by Chamel (e.g., [18]) that free neutrons in the inner neutron star crust are not actually free but are entrained by nuclei. In this case they increase the effective mass of the nuclei and decrease the ion plasma and cyclotron frequencies. By doing this at given T they make the crystal less quantum and thus increase its specific heat. We have included this effect by adopting the fraction of entrained neutrons from Tab. I in [18]. The result (dotted, green curve "ent" in Fig. 4d) is the dramatic increase of the specific heat comparable to that of the superstrong magnetic field in the standard model without neutron entrainment.

5. Binary Coulomb crystals

The last topic of this work is binary Coulomb crystals. This subject may be important for the white dwarf cores, where one has CO mixture, and also for the neutron star crusts, where one can expect various mixtures at various densities. In this work the one-to-one ratio of two constituents is assumed as well as their ordered distribution over nodes of a bcc lattice (Fig. 5a). This structure has to be treated as a simple cubic lattice with 2 different ions in the elementary cell. The BZ of this lattice is a cube. According to [19] such a crystal is unstable if the charge ratio is ≥ 3.6 irrespective of the mass ratio.

As in Sect. 2 one can construct the dynamic matrix and solve the respective secular equation at every point **k** of the BZ to find phonon frequencies [19]. In this case there are

6 frequencies at each $\mathbf{k}$, which satisfy a modified Kohn's sum rule $\sum_{i=1}^{6}\omega_i^2 = 2\omega_{\rm s}^2$, where $\omega_{\rm s} = T_{\rm s}/\hbar = \sqrt{\pi n e^2(Z_1+Z_2)(Z_1/M_1+Z_2/M_2)}$ is the binary mixture plasma frequency (n is the number density of all ions). In Fig. 5b, 3 sets of dispersion curves are plotted in the direction (211) up to the BZ boundary in this direction. The solid (red) curves correspond to identical ions while dotted (black) curves show dispersion relations of a bcc lattice of identical ions in the same direction. Naturally, solid and dotted curves coincide but the dotted ones can be extended further (cf. Fig. 1a), up to the boundary of the bcc lattice BZ. The dot-dashed (blue) and dashed (green) curves correspond to charge and mass ratios of 3, respectively.

It is customary to obtain thermodynamic functions of any mixture from the so-called linear mixing theory, in which, say, the binary mixture total heat capacity is $C_{\rm lm} = N_1c_1 + N_2c_2$, where N_i is the total number of particles of the i-th type and c_i is the specific heat of the system composed only of the i-th ion species at the same temperature and electron number density as in the mixture. But now we know the exact frequencies of the ordered binary crystal mixture and thus are in a position to calculate its exact specific heat $C_{\rm bin}$ [19]. This allows one to assess the validity of the linear mixing theory for application to such mixtures.

In Fig. 5c we plot the ratio of the linear mixing specific heat to the exact binary crystal specific heat. At high temperatures the linear mixing theory reproduces the Dulong-Petit law and consequently is very accurate. But at low temperatures it overestimates the specific heat substantially. For instance, by 80% for iron/oxygen mixture and by almost 30% for CO mixture [19, 2]. This will affect quantitatively the cooling curves of white dwarfs and may be important for modeling neutron star crust thermal relaxation if this structure is realized.

6. Conclusion

The work on Coulomb crystal theory continues. For the sake of white dwarf cooling theory it is desirable to calculate the crystal anharmonic energy in quantum regime (only classic crystal anharmonic energy is currently known). It is also worthwhile to study Coulomb crystal mixtures with substitutional disorder. Both topics are currently work in progress.

Acknowledgments

The author is grateful to D.G. Yakovlev and A.A. Kozhberov for discussions. This work was partially supported by RFBR (grant 14-02-00868) and by Rosnauka (grant NSh 294.2014.2).

References

[1] Haensel P, Potekhin A Y and Yakovlev D G 2007 *Neutron Stars 1: Equation of State and Structure* (New York: Springer)
[2] Kozhberov A A and Baiko D A *in preparation*
[3] Baiko D A 2000 Ph.D. thesis, A.F. Ioffe Physical–Technical Institute
[4] Baiko D A, Potekhin A Y and Yakovlev D G 2001 *Phys. Rev.* E **64** 057402
[5] Fuchs K 1936 *Proc. Roy. Soc. London* **153** 622
[6] Baiko D A 2011 *Mon. Not. Roy. Astron. Soc.* **416** 22
[7] Landau L D and Lifshitz E M 1980 *Statistical Physics. Part I* (Oxford: Pergamon Press)
[8] Landau L D and Lifshitz E M 1986 *Theory of Elasticity* (Oxford: Pergamon Press)
[9] Wallace D C 1967 *Phys. Rev.* **162** 776
[10] Ogata S and Ichimaru S 1990 *Phys. Rev.* A **42** 4867
[11] Jancovici B 1962 *Nuovo Cimento* **25** 428
[12] Baiko D A 2002 *Phys. Rev.* E **66** 056405
[13] Pollock E L and Hansen J P 1973 *Phys. Rev.* A **8** 3110
[14] Landau L D and Lifshitz E M 1975 *The Classical Theory of Fields* (Oxford: Pergamon Press)
[15] Baiko D A 2009 *Phys. Rev.* E **80** 046405
[16] Baiko D A and Yakovlev D G 2013 *Mon. Not. Roy. Astron. Soc.* **433** 2018
[17] Usov N A, Grebenschikov Yu B and Ulinich F R 1980 *J. Exp. Theor. Phys.* **78** 296
[18] Chamel N 2012 *Phys. Rev.* C **85** 035801
[19] Kozhberov A A and Baiko D A 2012 *Contrib. Plasma Phys.* **52** 153